Scientific Papers. Series E. Land Reclamation, Earth Observation & Surveying, Environmental Engineering. Vol. XV, 2026
Print ISSN 2285-6064, CD-ROM ISSN 2285-6072, Online ISSN 2393-5138, ISSN-L 2285-6064

SATELLITE-DERIVED TURBIDITY AS AN INDICATOR OF SMALL-SCALE GOLD MINING ACTIVITY AROUND THE BROKOPONDO RESERVOIR, SURINAME

Tamara MYSLYVA[1], Christiaan Max HUISDEN[1], Marek MROZ[2], Gerald TJON A SAN[1], Fauzia Gatoen ABDOELRAHMAN[3]

[1]Anton de Kom University of Suriname, 86 Leysweg, Paramaribo, Republic of Suriname
[2]University of Warmia and Mazury in Olsztyn, 1 Michała Oczapowskiego Str., 10-719, Olsztyn, Poland
[3]Ministry of Foreign Affairs, International Business and Cooperation, 8 Henck Arronstraat, Paramaribo, Republic of Suriname

Corresponding author email: byrty41@yahoo.com

Abstract

The rapid expansion of illegal gold mining over the past decade has emerged as one of the most critical environmental challenges in Suriname, driven by its severe impacts on both terrestrial and aquatic ecosystems. Monitoring these activities is difficult due to the remoteness of affected areas, limited accessibility, and safety constraints. This study explores the potential of Sentinel-2 Level-2A imagery for detecting and monitoring artisanal and small-scale gold mining (ASGM) activity around the Brokopondo Reservoir without relying on in-situ measurements. A Python-based workflow developed in Google Colab was used to pre-process the imagery and calculate the Normalized Difference Turbidity Index (NDTI) for the period 2021–2025. Spatial relationships between high and low NDTI clusters and their proximity to ASGM sites were examined using Moran's I, the Mann–Whitney U test, and Cliff's delta. The results suggest that NDTI has potential as a remote-sensing proxy for ASGM-related water turbidity, offering valuable support for environmental monitoring in remote tropical forest regions of the Guiana Shield.

Key words: *gold mining activity, indication, monitoring, proximity, water turbidity.*

INTRODUCTION

Artisanal and small-scale gold mining (ASGM) is a critical livelihood activity in Suriname, supporting an estimated 20,000 people, particularly in interior regions such as Brokopondo and Sipaliwini (Seccatore & Theije, 2017; First National Action Plan, 2023). Although the sector contributes significantly to local economies, it also generates substantial environmental and public health risks due to the use of hazardous substances, especially mercury, during gold extraction (Marshall et al., 2020; Quispe Aquino et al., 2022; Malone et al., 2023). The environmental footprint of mercury use in artisanal and small-scale gold mining is especially pronounced in riverine and reservoir systems adjacent to mining areas, where disturbed soils and associated contaminants are mobilized into waterways, resulting in water quality degradation (Huisden et al., 2021). ASGM in Suriname primarily relies on hydraulic mining techniques that remove vegetation and mobilize large volumes of soil and sediment. These materials are commonly discharged directly into nearby rivers and creeks without sediment-control structures such as tailings ponds (Heemskerk & Kooye, 2003; Ouboter, 2015). The influx of fine sediments increases turbidity and facilitates the downstream transport of mercury-contaminated particles, as mercury readily binds to clay and fine sediment (Vreedzaam et al., 2023).

The Brokopondo Reservoir is located within one of Suriname's most active artisanal and small-scale gold mining regions, the Brokopondo district. Mining is a major driver of deforestation and ecological degradation in this area, with much of the activity occurring illegally (Global Forest Watch, 2025). Elevated sediment loads and turbidity within the reservoir and its tributaries have been directly linked to mining operations, posing risks to aquatic ecosystems and communities that rely on the water for

drinking, fishing, and other livelihood activities (Heemskerk et al., 2022). Despite the severity of ASGM-related environmental impacts, Suriname lacks a national system for systematic monitoring of water quality or mining activities (Rodríguez & Chavez, 2024). Reliable data on the extent and distribution of ASGM, particularly in the Brokopondo district, are limited (EMSAGS, 2023). Many mining sites are located in remote forested areas that are difficult to access and may pose safety risks for field researchers (United Nations Office on Drugs and Crime, 2025). These logistical and security constraints severely limit the feasibility of routine field sampling and make traditional monitoring approaches impractical in many ASGM-affected regions. Given these constraints, remote sensing provides a practical and effective alternative to ground-based monitoring.

Satellite imagery offers consistent, high-resolution, and high-frequency observations that enable the assessment of spatial and temporal variations in water quality where field measurements are not feasible (Espinoza et al., 2025). Sentinel-2, with its suitable spectral configuration and frequent revisit time, has become a widely used platform for monitoring optically complex inland waters (Elhag et al., 2019; Das et al., 2024). A substantial body of literature demonstrates that multispectral indices serve as reliable proxies for water-quality parameters such as turbidity (Steinbach et al., 2025), suspended sediment concentration (SSC), total suspended matter (TSM), chlorophyll-a (Chl-a), and coloured dissolved organic matter (CDOM) (Khan et al., 2021; Li et al., 2023; Chen et al., 2024; Tesfaye, 2024). Red–green reflectance contrasts are particularly effective in detecting sediment-laden waters associated with mining disturbances.

The Normalized Difference Turbidity Index (NDTI), derived from red and green spectral bands, has emerged as a robust indicator of relative turbidity and suspended sediments in both inland and coastal waters (Zhang et al., 2022; Amran & Daming, 2023). In river systems affected by ASGM, persistent turbidity hotspots downstream of mining areas provide strong qualitative evidence of sediment release even when in situ turbidity measurements are unavailable (Sousa & Veiga, 2009; Pereira & Lobo, 2024). Because many ASGM sites in Suriname are located in remote forested landscapes, including protected and Indigenous territories, satellite-based turbidity assessment is often the only feasible large-scale monitoring option. Remote sensing of water turbidity therefore offers a crucial means of detecting and understanding ASGM-induced sediment dynamics across the Brokopondo Reservoir and the broader Guiana Shield.

The purpose of this study is to evaluate the feasibility of using the Normalized Difference Turbidity Index, derived from Sentinel-2 imagery, as an indirect indicator of artisanal and small-scale gold mining activity around the Brokopondo Reservoir in Suriname in the absence of field-based water quality measurements. By generating multi-year, dry-season NDTI composites and analysing their spatial and temporal patterns, the study aims to determine whether elevated turbidity signals (NDTI hotspots) correspond spatially with known ASGM locations and can therefore be evaluated as a potential tool for environmental monitoring in remote, data-poor regions.

This study pursues five interconnected objectives: (1) to generate a spatial-temporal dataset of NDTI values for the Brokopondo Reservoir and its tributaries using Sentinel-2 imagery from 2021 to 2025, focusing on the dry-season months (July-November) when turbidity signals are most stable and comparable; (2) to characterize spatial turbidity using spatial autocorrelation methods, including Global Moran's I and Local Moran's I, in order to identify statistically significant clusters of high (HH) and low (LL) NDTI values across the study area; (3) to quantify the spatial relationship between ASGM sites and NDTI clusters by calculating distances from known ASGM locations to HH and LL clusters and evaluating whether mining sites are preferentially located near turbidity hotspots; (4) to statistically assess differences in proximity between ASGM sites and NDTI cluster types using the Mann-Whitney U test and Cliff's delta effect size, thereby testing the hypothesis that ASGM sites are significantly closer to HH clusters than to LL clusters; (5) to evaluate the potential of NDTI as a field-independent proxy for monitoring ASGM impacts, providing a scalable, replicable method for environmental surveillance in regions where ground-based

water quality monitoring is logistically constrained or unavailable.

MATERIALS AND METHODS

Study area. The study was conducted in Suriname, a country situated north of the equator on the north-eastern coast of South America. Suriname's geographical coordinates extend from 1°50.45' N to 6°0.35' N and from 53°59.08' W to 54°33.49' W. Geologically, more than 80% of Suriname consists of the deeply weathered, rainforest-covered Precambrian Guiana Shield (Myslyva et al., 2024).

The area of interest is the Brokopondo Reservoir, officially known as the Professor Doctor Ingenieur W. J. van Blommestein Meer, also referred to as Brokopondostuwmeer (Leentvaar, 1975). It was formed in the 1960s following the construction of the Afobaka Dam on the Suriname River. The reservoir was primarily created to supply hydroelectric power to support the country's bauxite industry and general electricity needs. With a surface area that fluctuates around 1,560 km² depending on seasonal water levels, and catchment area approximately 12,200 km², it ranks among the largest human-made reservoirs in South America. The reservoir alone covers nearly one percent of Suriname's total land area. It lies in the Brokopondo district and extends between latitudes 4°20' N and 5°00' N and longitudes 54°50' W and 55°20' W (Figure 1).

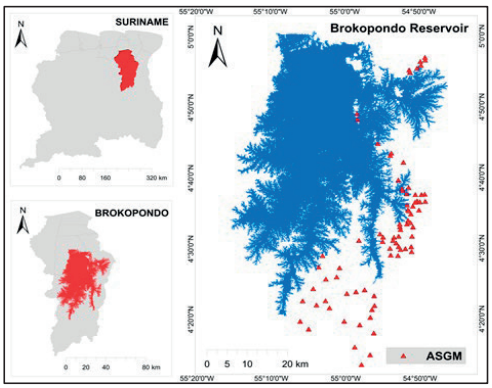


Figure 1. Location of the study area

The reservoir and its catchment are subject to various human activities, including artisanal and small-scale gold mining, agriculture, and logging, all of which affect water quality and sediment dynamics. Its size, hydrological characteristics, and environmental pressures make the Brokopondo Reservoir an important focus for remote sensing studies aimed at monitoring water turbidity, sediment transport, and land-use changes in tropical reservoirs.

The region of interest included the Brokopondo Reservoir and a 25-km buffer zone surrounding its shoreline. This extent was sufficiently large to capture the major tributaries and first-order streams flowing into the reservoir, as well as the majority of direct-impact ASGM sites and their associated drainage pathways. To estimate proximity to high-high (HH) and low-low (LL) water turbidity clusters, 80 ASGM activity points were selected.

Figure 2 presents a step-by-step methodological framework used to validate the application of the Normalized Difference Turbidity Index as an indicator of artisanal and small-scale gold mining activity by analyzing the spatial proximity of ASGM sites to major NDTI clusters within the Brokopondo Reservoir. The workflow integrates remote sensing, spatial autocorrelation analysis, proximity assessment, and statistical validation using the Mann-Whitney U test and Cliff's delta to quantify the association between ASGM activity and water turbidity patterns.

Datasets used. This study employed Sentinel-2 Level-2A surface reflectance imagery obtained from the harmonized collection available on the Google Earth Engine (GEE) platform. This dataset provides atmospherically corrected reflectance at 10-20 m spatial resolution and includes consistent radiometric calibration across the mission. Details of the other datasets used in this study are provided in Table 1.

Table 1. Characteristics of data collected

Data	Source	Acquisition year	Scale/ Resolution
Digital Elevation Model (DEM)	30-Meter SRTM Tile Downloader: https://dwtkns.com/srtm30m/	2018	1-arcsecond (3601x 3601 pixels)
Shape-file with locations of gold mining activity	National Environmental Authority: https://nimos.org/en/about-us/	2018	–
Shapefile of the Brokopondo Reservoir boundary	National Land Monitoring System of Suriname (GONINI) https://www.gonini.sbb.sr/	2023	–

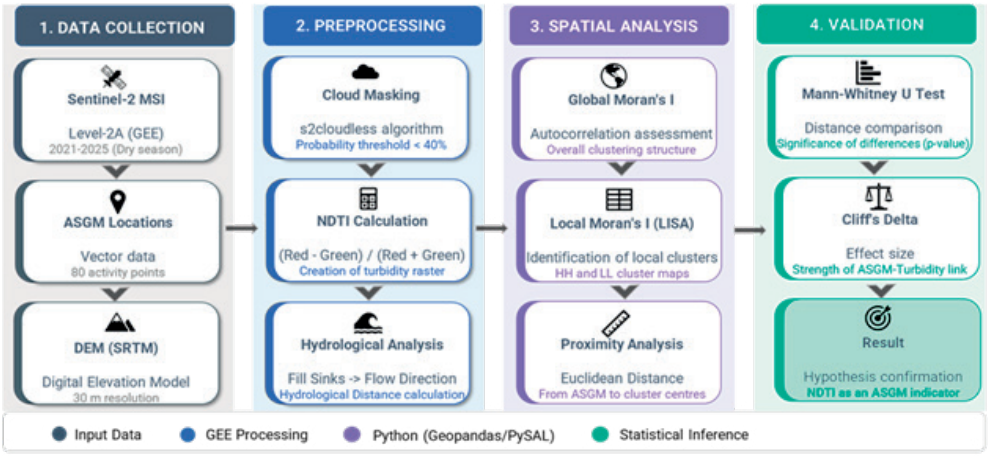


Figure 2. Overall scheme of the methodological approach for the research

The imagery was spatially filtered to the region of interest (ROI) covering the Brokopondo Reservoir and temporally constrained to the period from January 2021 to October 2025. A vector mask derived from a shapefile delineating the official boundaries of the Brokopondo Reservoir, obtained from the National Land Monitoring System of Suriname (GONINI), was used to define the reservoir extent. To exclude the influence of precipitation on water turbidity in the reservoir, only images acquired during July – November were retained.

Cloud masking approach. To minimize atmospheric contamination, all Sentinel-2 Level-2A surface reflectance data were corrected for cloud interference using the *s2cloudless* cloud-probability algorithm. The *s2cloudless* model is a machine-learning system based on gradient-boosted decision trees developed by ESA and Sinergise specifically for Sentinel-2 optical imagery. It generates a pixel-level cloud probability map (0-100%) provided in the COPERNICUS/S2_CLOUD_PROBABILITY dataset, which is temporally aligned with the Sentinel-2 SR image collection.

In this workflow, the cloud-probability band was added to each Sentinel-2 image by matching acquisition times. Cloud masking was performed using a probability-threshold approach commonly applied in Sentinel-2 pre-processing. Specifically, pixels with a cloud probability ≥ 40% were flagged as cloud-contaminated and removed from further analysis, while pixels with a probability < 40% were retained (GEE tutorial, 2025).

Water turbidity index computation. To quantify water turbidity, the Normalized Difference Turbidity Index (NDTI) was calculated for each cloud-free Sentinel-2 scene. NDTI is defined as:

$$NDTI = \frac{(R_{red} - R_{green})}{(R_{red} + R_{green})} \quad (1)$$

where R_{Red} corresponds to Sentinel-2 Band 4 (665 nm) and R_{Green} corresponds to Band 3 (560 nm) (Dewantoro et al., 2024).

This index is based on the relationship between turbidity and the spectral response of surface waters, where higher turbidity generally corresponds to higher NDTI values and vice versa. The index uses green and red band reflectance to estimate variations in suspended sediment concentration within the water column. This band combination effectively discriminates sediment-laden water; therefore, NDTI serves as a key indicator for turbidity mapping (Foteh et al., 2018).

NDTI was calculated for each selected scene and exported as raster layers for subsequent analysis.

Based on Sentinel-2 spectral characteristics and the typical optical behaviour of tropical inland waters, NDTI values were interpreted as follows: (i) NDTI < −0.1 – indicates clear water conditions, where green reflectance dominates (these values are typical of low suspended sediment concentrations and may occur in calm

reservoir areas, isolated ponds, or waters influenced by biological activity rather than mineral turbidity); (ii) −0.1 ≤ NDTI ≤ 0.1 – indicates low to moderate turbidity or transitional conditions, where red and green reflectance are comparable (this range is commonly observed in relatively stable reservoir waters with limited sediment input); (iii) < NDTI ≤ 0.3 – indicates moderate turbidity, often associated with increased suspended inorganic particles (such values may reflect seasonal runoff, shoreline disturbance, or early-stage mining impacts); (iv) NDTI > 0.3 – indicates high turbidity, dominated by mineral suspended matter (in the Brokopondo Reservoir, such values are consistent with sediment-laden inflows from upstream rivers and creeks affected by artisanal and small-scale gold mining activity).

Hydrological distance calculation. Hydrological distance was computed using ArcGIS 10.8 Hydrology toolbox to quantify flow-path connectivity within the Brokopondo Reservoir system. First, the digital elevation model was hydrologically corrected by filling sinks to ensure a continuous flow surface. Flow direction was then derived using the D8 algorithm, followed by flow accumulation to represent potential drainage pathways. Based on these layers, the stream identification step was used to delineate flow channels. The Flow Length tool was then applied in downstream mode to calculate the cumulative distance that water would travel along the flow network from each cell to the reservoir outlet.

The resulting hydrological distance raster represents a process-based metric of spatial connectivity constrained by the drainage network and was subsequently used in spatial statistical analyses to interpret the distribution, clustering, and downstream propagation of NDTI-derived turbidity signals.

Global and Local Moran's Index calculations. Spatial autocorrelation of the water turbidity values was assessed using Global Moran's I and Local Moran's I (LISA) statistics. These indices evaluate whether high or low values are spatially clustered or randomly distributed.

The *Global Moran's I* index provides a single summary statistic describing the overall spatial structure of the dataset. It was calculated following Mitchell (2005) using:

$$I = \frac{n}{\sum_{i=1}^{n}\sum_{j=1}^{n} w_{ij}} \cdot \frac{n\sum_{i=1}^{n}\sum_{j=i}^{n} w_{ij}(y_i-\bar{y})(y_j-\bar{y})}{\sum_{i=1}^{n}(y_i-\bar{y})^2]} \quad (2)$$

where n represents the number of spatial units; y_i is the attribute value at location i; $\bar{y}$ is the mean of the attribute and w_{ij} is the spatial weight between locations i and j.

Values of Moran's I greater than zero indicate positive spatial autocorrelation (clustering of similar values), values below zero indicate negative spatial autocorrelation (dispersion), and values near zero indicate spatial randomness.

Local Moran's I was applied to detect local clusters and spatial outliers, providing insight into the spatial heterogeneity of turbidity patterns. The Local Moran's I statistic for each location i was computed as follows:

$$I_i = \frac{(y_i-\bar{y})}{m_2}\sum_{k=1}^{n} w_{ij}(y_j - \bar{y}) \quad (3)$$

where the normalization term m_2 is:

$$m_2 = \frac{1}{n}\sum_{k=1}^{n}(y_k - \bar{y})^2 \quad (4)$$

Positive and statistically significant I_i values indicate HH or LL clusters, while negative values represent HL or LH outliers. This enables the identification of areas with anomalous turbidity behaviour within the reservoir.

Statistical evaluation of ASGM-turbidity relationships. The non-parametric Mann-Whitney U test was used to determine whether high-high turbidity clusters are significantly closer to ASGM sites than low-low clusters representing relatively clean-water areas. This test was selected because the distance data showed non-normal distributions and unequal variances, making non-parametric inference more appropriate than parametric alternatives. To complement the significance testing, Cliff's delta (δ) was calculated as a measure of effect size. Cliff's delta quantifies the probability that a randomly selected value from one group will exceed a randomly selected value from another group, minus the reverse probability. As a distribution-free statistic, it is well suited for skewed data, unequal sample sizes, and non-parametric comparison frameworks such as the Mann–Whitney test (Vargha & Delaney, 2000). Interpretation followed established thresholds,

where $\delta < 0.147$ indicates a negligible effect, $0.147 \leq \delta < 0.33$ a small effect, $0.33 \leq \delta < 0.474$ a medium effect, and $\delta \geq 0.474$ a large effect (Romano et al., 2006). Together, these metrics provide a robust assessment of both the statistical significance and the magnitude of differences between cluster types in relation to ASGM proximity.

Software and computational workflow. All image pre-processing, index computation, and spatial-statistical analyses were conducted in Google Colab (Python environment). Sentinel-2 imagery was accessed and processed using the Google Earth Engine Python API in combination with *geemap* and *xee*, enabling cloud-based filtering, cloud masking, and surface reflectance compositing.

Spatial data handling and vector operations were performed using *GeoPandas*, *Shapely*, and *STRtree*, while raster manipulation and masking were conducted with *rasterio* and *xarray*. Distance metrics, including hydrological distance and Euclidean distance between ASGM point locations and cluster pixels, were generated using *NumPy* and raster/vector spatial indexing routines. Non-parametric statistical testing was performed using *SciPy*.

RESULTS AND DISCUSSIONS

A time series of NDTI maps spanning July 2021 to October 2025 reveals distinct cyclical patterns in the spatial distribution of water turbidity across the Brokopondo Reservoir (Figure 3).

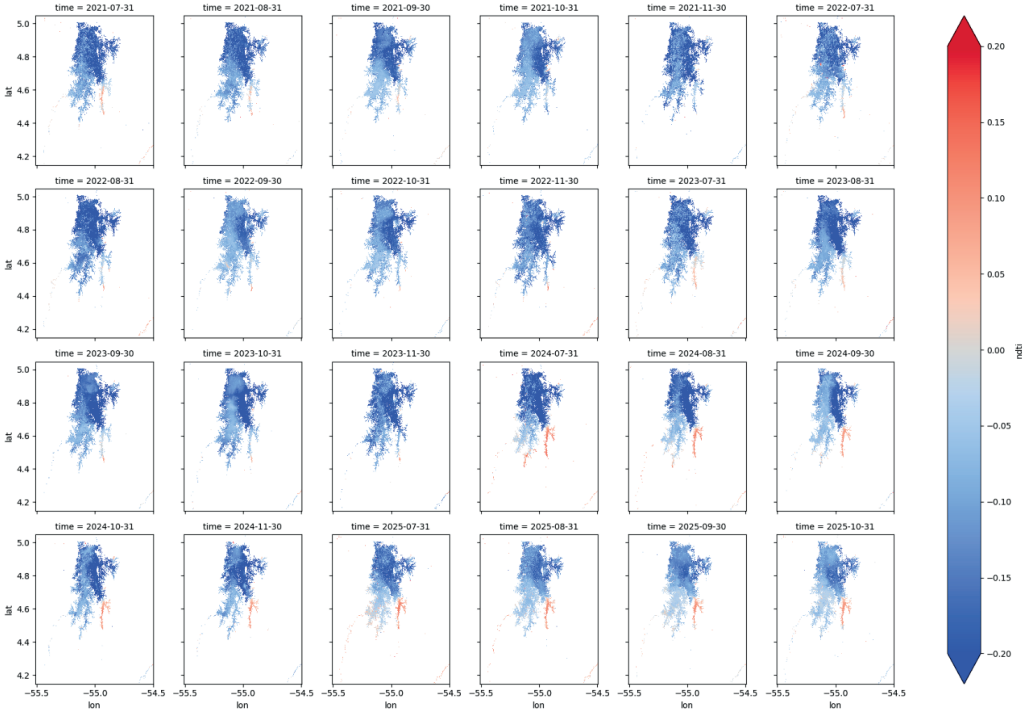


Figure 3. NDTI values and distribution for the Brokopondo Reservoir

The southern portion of the reservoir consistently exhibits the highest turbidity levels throughout the five-year period, corresponding to areas of intensive artisanal and small-scale gold mining activity. Temporal analysis indicates significantly lower turbidity during July 2021-November 2022 compared to July 2024-October 2025.

The suppressed turbidity observed in 2021 is likely a direct consequence of COVID-19 lockdown measures in Suriname, which restricted ASGM operations by limiting access to essential inputs such as fuel, equipment, and mercury used for amalgamation. Similarly, the reduced turbidity observed from July to November 2022 is associated with extreme

hydrological events. Unseasonably heavy rainfall in January and February 2022 – months typically classified as part of the short dry season – necessitated the controlled release of water from the Afobaka Dam on 28 February to mitigate rising reservoir levels. By 15 March, the resulting floods had propagated into the Upper Suriname, Tapanahoni, Lawa, and Marowijne river catchments, disrupting both mining operations and material transport. These hydrological disturbances temporarily curtailed gold mining activity and sediment mobilization from mining sites, as reflected in the NDTI-derived turbidity patterns. In contrast, the elevated turbidity observed in 2024-2025 corresponds to resumed and intensified ASGM activity under normal hydrological conditions, highlighting the strong coupling between anthropogenic sediment inputs and reservoir turbidity.

Considering these contextual factors, the period from July 2024 to October 2025 was selected for subsequent analysis, as it represents a more stable phase in which turbidity variations are more likely to reflect mining-related impacts rather than exceptional climatic or operational disruptions.

Global Moran's I was calculated to quantify the overall spatial structure of the NDTI dataset (Table 2).

Table 2. Spatial autocorrelation of NDTI-derived turbidity in the Brokopondo Reservoir based on Global Moran's I (July 2024-October 2025)

Date	Global Moran's I	z-score	p-value
July 2024	0.834004	422.5635	< 0.0001
August 2024	0.854091	429.6744	< 0.0001
September 2024	0.812478	410.3696	< 0.0001
October 2024	0.821867	412.3634	< 0.0001
November 2024	0.82093	415.7692	< 0.0001
July 2025	0.869067	442.2297	< 0.0001
August 2025	0.810761	415.0792	< 0.0001
September 2025	0.838833	424.9217	< 0.0001
October 2025	0.799329	405.948	< 0.0001

This indicator demonstrates consistently very strong and statistically significant positive spatial autocorrelation of NDTI-derived turbidity patterns across the Brokopondo Reservoir for all analyzed months between July 2024 and October 2025. Moran's I values range from 0.799 to 0.869, close to the theoretical upper limit of +1, indicating that high and low turbidity values are strongly clustered in space rather than randomly distributed.

The extremely high z-scores (405.9 to 442.2) and p-values < 0.0001 confirm that these clustering patterns are highly unlikely to have occurred by chance. The strongest spatial clustering was observed in July 2025 (I = 0.869), while slightly lower – but still very strong – clustering occurred in October 2025 (I = 0.799). These results suggest that sediment-rich and sediment-poor zones remain spatially stable over time. The strength and persistence of these spatial patterns support the suitability of NDTI as a robust indicator for identifying and monitoring persistent turbidity hotspots potentially linked to ASGM activity.

After confirming significant spatial clustering in the dataset, Local Moran's I was calculated to identify the spatial distribution of high and low NDTI values and to delineate HH and LL clusters, as well as spatial outliers (HL and LH) (Table 3).

Table 3. Non-parametric test statistics for spatial NDTI HH and LL cluster differentiation (July 2024-October 2025)

Date	U statistic	p-value	Cliff's delta (effect size)
July 2024	284080.0	< 0.000001	1.0
August 2024	5606522.0	< 0.000001	1.0
September 2024	4997040.0	< 0.000001	1.0
October 2024	4105832.0	< 0.000001	1.0
November 2024	3652980.0	< 0.000001	1.0
July 2025	6580161.0	< 0.000001	1.0
August 2025	6075216.0	< 0.000001	1.0
September 2025	6224660.0	< 0.000001	1.0
October 2025	6107759.0	< 0.000001	1.0

The Mann-Whitney U test results comparing HH and LL clusters reveal extremely strong and highly consistent differences between the two groups across all analyzed months. U statistics range from 284,080 (July 2024) to 6,580,161 (July 2025), with all pairwise comparisons yielding p-values < 0.000001, indicating robust statistical separation between the distributions.

Notably, Cliff's delta equals 1.0 for every month, representing the maximum possible effect size and demonstrating complete non-overlap between HH and LL cluster values. This uniform pattern indicates highly stable and persistent spatial differentiation of NDTI across both dry-season periods (2024 and 2025).

HH clusters consistently represent markedly higher turbidity-related index values, while LL

clusters represent persistently low values, with no intermediate overlap. Such effect sizes confirm that the spatial clustering of NDTI is both statistically significant and structurally robust.

Using the NDTI as an indicator of ASGM activity is a promising approach, but it has important limitations. In the Brokopondo Reservoir, increased water turbidity is not caused solely by gold mining; it can also be influenced by natural factors such as rainfall intensity, surface runoff, and local topography. To minimize precipitation-related effects, the analysis was restricted to the regional dry season (July-November), with particular emphasis on the driest months (September-November), consistently observed during 2021-2025. This temporal filtering allowed the analysis to focus on periods when anthropogenic sediment inputs from ASGM were less masked by rainfall-driven turbidity. A statistical assessment of the relationship between NDTI and precipitation for July 2021 – October 2025 showed a very weak correlation (Pearson's r = 0.08), indicating negligible linear dependence between rainfall and turbidity during the selected dry-season periods (Figure 4).

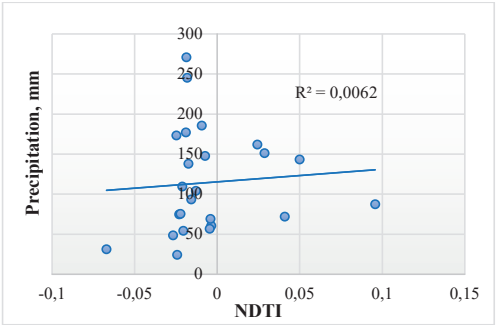


Figure 4. Relationship between NDTI and precipitation (2021-2025)

This weak correlation suggests that precipitation was not a dominant driver of turbidity variability within the area of interest during the analyzed periods, supporting the interpretation that the observed turbidity patterns are largely associated with anthropogenic disturbance.

To evaluate the influence of topography on turbidity patterns, hydrological distance was calculated and its relationship with the spatial distribution of high-high (HH) and low-low (LL) clusters were analysed (Table 4).

Table 4. Non-parametric test statistics for spatial relationships between NDTI clusters and hydrological distance (July 2024-October 2025)

Date	U statistic	p-value	Cliff's delta (effect size)
July 2024	116882.0	< 0.000001	-0.1771
August 2024	2617028.5	0.000053	-0.0664
September 2024	2341722.0	0.000171	-0.0628
October 2024	1872022.5	< 0.000001	-0.0881
November 2024	1533951.0	< 0.000001	-0.1602
July 2025	2858760.0	< 0.000001	-0.1311
August 2025	2613307.0	< 0.000001	-0.1397
September 2025	2955452.0	0.001388	-0.0504
October 2025	2884479.0	0.000454	-0.0555

The non-parametric test results revealed no meaningful relationship between the spatial distribution of HH and LL clusters and hydrological distance. Although several months show statistically significant p-values, all Cliff's delta values are small and negative (–0.05 to – 0.18), indicating negligible effect sizes and confirming the absence of a systematic spatial trend. This means that neither HH nor LL clusters align with the longitudinal hydrological gradient of the reservoir. High-turbidity areas do not consistently occur upstream or downstream, and low-turbidity areas are not preferentially located farther from inflows. Instead, turbidity clusters appear spatially patchy and locally constrained, suggesting that hydrological distance is not a meaningful predictor of turbidity distribution. These results indicate that turbidity dynamics in the Brokopondo Reservoir are driven primarily by localized factors – such as ASGM activity, shoreline erosion, and small tributaries – rather than by overall hydrological connectivity.

To achieve the research objective, a proximity analysis was conducted to examine the relationship between high-intensity pollution sources (ASGM) and high-intensity effects (NDTI clusters). Euclidean distances were calculated from each ASGM location to all HH and LL cluster points within a 25 km zone around the Brokopondo Reservoir (Table 5).

Because field turbidity measurements were unavailable, nonparametric methods were used instead of regression modelling. The Mann–Whitney U test and Cliff's delta were applied to assess whether HH clusters are significantly closer to ASGM sites than LL clusters.

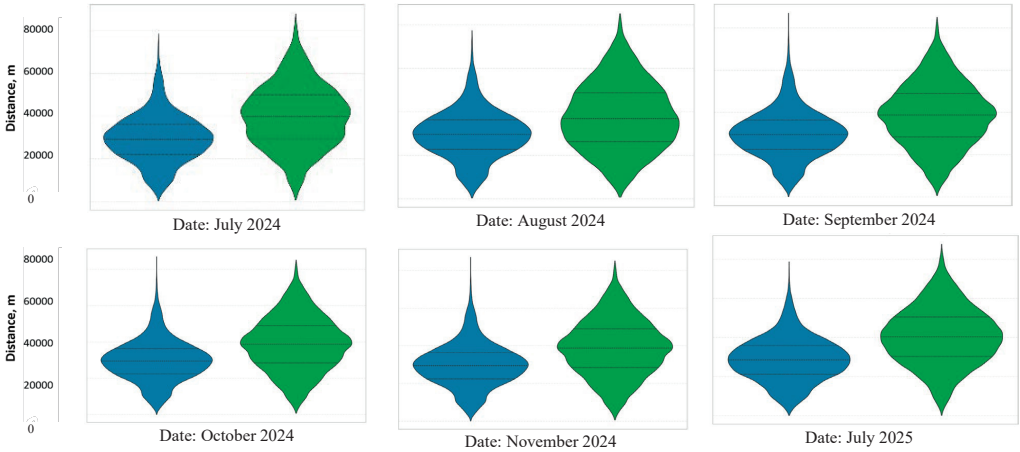
Across all months, HH clusters were consistently closer to ASGM sites than LL clusters. Mean distances ranged from 28,855 m to 30,798 m for HH clusters and from 37,791 m to 40,770 m for LL clusters.

U statistic and corresponding p-values (all p = 0.01) indicate statistically significant differences each month. Cliff's delta values were consistently negative (−0.3046 to −0.4715), confirming that ASGM locations are spatially associated with HH clusters rather than LL clusters. This pattern suggests a robust spatial correlation between areas of increased turbidity and proximal ASGM activity, supporting the use of NDTI clustering as an indicator for mining-related water quality impacts.

The violin plots (Figure 5) show a clear spatial separation between water turbidity cluster types and their proximity to artisanal and small-scale gold mining sites. Areas classified as high-high turbidity clusters are located, on average, at considerably smaller distances from ASGM operations compared to low-low turbidity clusters. This spatial relationship confirms the assumption that gold mining proximity is the primary driver of elevated sediment loads in the Brokopondo Reservoir.

Table 5. Distances between all ASGM locations and all HH and LL clusters points (July 2024-October 2025)

Date	Cluster	Distance, m			U statistic	p-value	Cliff's delta (effect size)
		min	max	mean			
July 2024	HH	452	78560	29558	32565897	0.01	-0.4268
	LL	778	87877	40039			
August 2024	HH	452	77395	29666	32754352	0.01	-0.3046
	LL	778	85146	37791			
September 2024	HH	244	78560	30209	663979890	0.01	-0.3356
	LL	497	87886	39076			
October 2024	HH	155	86971	29808	513405855	0.01	-0.3748
	LL	779	85066	38905			
November 2024	HH	155	88329	28916	435462823	0.01	-0.4040
	LL	497	84353	38370			
July 2025	HH	155	78853	28855	695519690	0.01	-0.4715
	LL	130	87886	40609			
August 2025	HH	155	78854	29644	682212917	0.01	-0.4385
	LL	518	88102	40696			
September 2025	HH	155	75740	29164	668830223	0.01	-0.4628
	LL	131	88102	40770			
October 2025	HH	155	78854	29598	721540967	0.01	-0.4093
	LL	131	88102	39606			



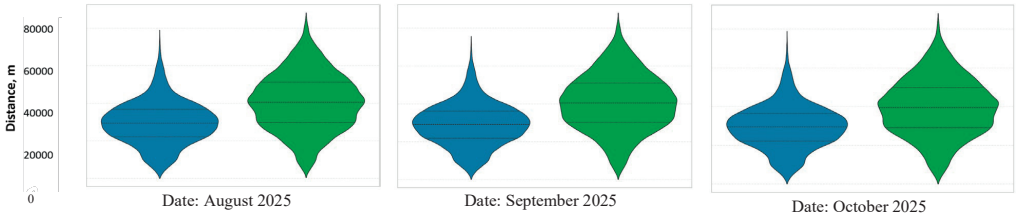


Figure 5. Violin plots showing the distribution of distances between ASGM sites and high–high (HH; blue) and low-low (LL; green) turbidity clusters

The results suggest that NDTI may provide an effective tool for identifying mining-related water turbidity. It relies solely on standard optical satellite imagery that is globally available, freely accessible, and frequently updated. Its calculation requires only red and green spectral bands, and is computationally simple and scalable. This makes it particularly valuable where field-based water quality data are limited or absent, enabling reproducible and cost-effective environmental monitoring of ASGM impacts in remote regions.

Future research could extend the proposed framework by integrating Land Surface Temperature (LST), the Normalized Difference Vegetation Index (NDVI), and the Bare Soil Index (BSI) with Normalized Difference Turbidity Index (NDTI)-based turbidity assessment. LST could provide complementary information on surface thermal changes associated with ASGM-related vegetation removal and soil exposure, while NDVI and BSI could help characterize vegetation loss and the expansion of disturbed or bare-soil areas around mining sites. Combining these indicators with NDTI could provide a more comprehensive assessment of the terrestrial–aquatic environmental footprint of ASGM and improve the monitoring of mining-induced landscape and water-quality changes.

CONCLUSIONS

This study provides a comprehensive spatiotemporal assessment of turbidity dynamics in the Brokopondo Reservoir and evaluates the suitability of the NDTI as a proxy for monitoring the impacts of artisanal and small-scale gold mining.

By integrating five years of dry-season Sentinel-2 observations with spatial statistics and proximity analyses, the research demonstrates that turbidity in the reservoir is strongly structured spatially, highly persistent over time, and closely associated with the distribution of mining activities. Global Moran's I values consistently close to +1 confirm pronounced and stable clustering of high and low turbidity zones across all analyzed months, while Local Moran's I results show clear spatial segregation between HH and LL clusters with complete non-overlap in their distributions. These findings indicate that turbidity hotspots are not randomly distributed but represent persistent spatial features.

The analysis further reveals that neither precipitation nor hydrological distance meaningfully explains turbidity variability during the dry-season months. The very weak correlation between NDTI and rainfall ($r = 0.08$) indicates that seasonal filtering effectively removed climate-driven noise from the dataset, while negligible effect sizes derived from the hydrological distance analysis demonstrate that turbidity patterns do not follow the longitudinal structure of the reservoir. Instead, turbidity clusters are spatially localized and strongly influenced by nearby anthropogenic disturbances.

The proximity analysis confirms a significant and consistent spatial association between ASGM sites and HH turbidity clusters. Across all months from 2024-2025, HH clusters were systematically located closer to mining areas than LL clusters, with statistically significant results and moderate to strong effect sizes. These outcomes provide robust empirical support for the hypothesis that ASGM is a primary driver of elevated turbidity in the Brokopondo Reservoir.

Overall, the study suggests that NDTI has potential as a scalable, field-independent proxy

for mining-related turbidity. Its reliance on freely available optical satellite data, minimal spectral inputs, and straightforward computation makes it a potentially valuable tool for environmental monitoring in remote regions where conventional water-quality measurements are limited or unavailable. By combining spatial clustering metrics, non-parametric statistics, and proximity analysis, this research establishes a reproducible framework for detecting and tracking ASGM impacts on freshwater systems. The methodology and results highlight the potential for NDTI-based monitoring to support decision-making in environmental governance, early warning systems, and long-term assessments of mining-driven landscape change in tropical watersheds.

REFERENCES

Amran, M., & Daming, W. (2023). Estimation of coastal waters turbidity using Sentinel-2 imagery. *Geodesy and Cartography*, 49(4), 180–185.

Chen, J., Wang, K., Li, X., Zhao, X., Cheng, X., Liu, Z., Zhang, J., & Zhang, S. (2024). Remote sensing inversion of water quality parameters (TSM, Chl-a, and CDOM) in subtidal seaweed beds and surrounding waters. *Ecological Indicators*, 167, 112716.

Das, S., Nandi, D., Thakur, R. R., Bera, D. K., Behera, D., Đurin, B., & Cetl, V. (2024). A novel approach for ex situ water quality monitoring using the Google Earth Engine and spectral indices in Chilika Lake, Odisha, India. *ISPRS International Journal of Geo-Information*, 13(11), 381.

Dewantoro, M. D. R., Ulfa, M., & Supatmanto, B. D. (2024). Water turbidity mapping using Sentinel-2A imagery and cloud-based Google Earth Engine in Saguling Reservoir. *IOP Conference Series: Earth and Environmental Science*, 1343(1), 012027.

Elhag, M., Gitas, I., Othman, A., Bahrawi, J., Gikas, P. (2019). Assessment of water quality parameters using temporal remote sensing spectral reflectance in arid environments. *Saudi Arabia. Water*, 11, 556.

EMSAGS Project. (2023). Final technical situational analysis: Artisanal and small-scale gold mining (ASGM) in Suriname (Final TSA report). EMSAGS / UNDP. Retrieved November 30, 2025, from https://emsags.org.

Espinoza, E., Baltodano, A., & Requena, N. (2025). Spatiotemporal analysis of water quality and optical changes induced by contaminants in lake Chinchaycocha Using Sentinel-2 and in situ data. *Water*, 17(15), 2195.

Foteh, R., Garg, V., Nikam, B. R., Khadatare, M. Y., Aggarwal, S. P., & Kumar, A. S. (2018). Reservoir sedimentation assessment through remote sensing and hydrological modelling. *Journal of the Indian Society of Remote Sensing*, 46, 1893–1905.

Global Forest Watch. (n.d.). Suriname. Retrieved November 30, 2025, from https://www.globalforestwatch.org.

Google Earth Engine tutorial. (n. d) Sentinel-2: Cloud masking with s2cloudless (community tutorial). Retrieved December 3, 2025, from https://developers.google.com.

Heemskerk, M. & Kooye, R. (2003). Challenges to Sustainable Small-Scale Mine Development in Suriname. 10.1201/9780203971284.ch36.

Heemskerk, M., Le Tourneau, F.-M., Hiwat, H., Cairo, H., & Pratley, P. (2022). In a life full of risks, COVID-19 makes little difference: Responses to COVID-19 among mobile migrants in gold mining areas in Suriname and French Guiana. *Social Science & Medicine*, 296, 114747.

Huisden, C. M., Landburg, G., Niram, A., Algoe, S., Dakriet, N. (2021) Mercury toxicity through fish consumption in Paramaribo, Suriname. *Academic Journal of Suriname*, (11)1, 25–32.

Khan, R. M., Salehi, B., Mahdianpari, M., & Mohammadimanesh, F. (2021). Water quality monitoring over Finger Lakes region using Sentinel-2 imagery on Google Earth Engine cloud computing platform. In ISPRS *Annals of the Photogrammetry, Remote Sensing and Spatial Information Sciences*, V-3-2021, 279–283.

Leentvaar, P. (1975). Hydrobiological observations in Surinam, with special reference to the manmade Brokopondo Lake. *Studies on the Fauna of Suriname and other Guyanas*, 15(56), 1–173.

Li, S., Kutser, T., Song, K., Liu, G., & Li, Y. (2023). Lake turbidity mapping using an OWTs-bp based framework and Sentinel-2 imagery. *Remote Sensing*, 15(10), 2489.

Malone, A., Figueroa, L., Wang, W., Smith, N. M., Ranville, J. F., Vuono, D. C., Alejo Zapata, F. D., Morales Paredes, L., Sharp, J. O., & Bellona, C. (2023). Transitional dynamics from mercury to cyanide-based processing in artisanal and small-scale gold mining: Social, economic, geochemical, and environmental considerations. *Science of the Total Environment*, 898, 165492.

Marshall, B. G., Veiga, M. M., da Silva, H. A. M., & Guimarães, J. R. D. (2020). Cyanide contamination of the Puyango-Tumbes River caused by artisanal gold mining in Portovelo-Zaruma, Ecuador. *Current Environmental Health Reports*, 7(3), 303–310.

Ministry of Natural Resources; National Institute for Environment and Development in Suriname (NIMOS); United Nations Development Programme (UNDP) (2023). First National Action Plan on Artisanal and Small-Scale Gold Mining (ASGM) in Suriname. EMSAGS Project. Retrieved December 5, 2025, from https://minamataconvention.org.

Mitchell, A. (2005). The ESRI Guide to GIS Analysis. *Esri Press*, 2.

Myslyva, T., Dasai, M., Huisden, C. M., Nadtochiy, P., Bilyavskyi, Y. (2024). Application of machine learning approaches for land use change modelling in Suriname. *Scientific Papers. Series E. Land Reclamation, Earth Observation and Surveying, Environmental Engineering*, 13, 830–840.

Ouboter, P. E. (2015). Review of mercury pollution in Suriname. *Academic Journal of Suriname*, 6, 531–543.

Pereira, B. M.& Lobo, F. d. L. (2024). Spatiotemporal analysis of total suspended solids in water bodies and mapping mining areas in Suriname and French Guiana. *Mining*, 4, 510–529.

Quispe Aquino, R., Malone, A., Smith, N. M., & García Zúñiga, F. F. (2022). Perceptions and realities of mercury contamination in a Peruvian artisanal and small-scale gold mining (ASGM) community. *Environmental Research*, 214, 114092.

Rodríguez, F., & Chavez, K. (2024). Small-scale gold mining study: Data to monitor environmental impacts in Suriname. Islamic Development Bank; Inter-American Development Bank; Global Partnership for Sustainable Development Data; Government of Suriname. Retrieved November 30, 2025, from https://www.data4sdgs.org.

Romano, J., Kromrey, J. D., Coraggio, J., Skowronek, J., & Devine, L. (2006). Exploring methods for evaluating group differences on the NSSE and other surveys: Are the t-test and Cohen's d indices the most appropriate choices? *Annual Meeting of the Southern Association for Institutional Research*.

Seccatore, J. & Theije, M. (2017). Socio-technical study of small-scale gold mining in Suriname. *Journal of Cleaner Production*, 144, 107–119.

Sousa, R. N., & Veiga, M. M. (2009). Using performance indicators to evaluate an environmental education program in artisanal gold mining communities in the Brazilian amazon. *Ambio*, 38, 40–46.

Steinbach, S., Bartels, A., Rienow, A., Thiongo, K., Zwart, S., & Nelson, A. (2025). Predicting turbidity dynamics in small reservoirs in central Kenya using remote sensing and machine learning. *International Journal of Applied Earth Observation and Geoinformation*, 136, 104390.

Tesfaye, A. (2024). Remote sensing-based water quality parameters retrieval methods: a review. *East African Journal of Environment and Natural Resources*, 7(1), 80-97.

United Nations Office on Drugs and Crime. (2025). Global analysis on crimes that affect the environment – Part 2b: Mineral's crime: Illegal gold mining. United Nations. Retrieved November 30, 2025, from https://www.unodc.org.

Vargha, A. & Delaney, H. D. (2000). A critique and improvement of the CL common language effect size statistics. *Journal of Educational and Behavioral Statistics*, 25(2), 101–132.

Vreedzaam, A., Ouboter, P. E., Hindori-Mohangoo, A. D., Lepak, R., Rumschlag, S., Janssen, S., Landburg, G., Shankar, A., Zijlmans, W., Lichtveld, M. Y., & Wickliffe, J. K. (2023). Contrasting mercury contamination scenarios and site susceptibilities confound fish mercury burdens in Suriname, *South America. Environmental Pollution*, 336, 122447.

Zhang, C., Liu, Y., Chen, X., & Gao, Y. (2022). Estimation of Suspended Sediment Concentration in the Yangtze Main Stream Based on Sentinel-2 MSI Data. *Remote Sensing*, 14(18), 4446.